CdS/activated carbon composite for the photocatalysis degradation of tetracycline hydrochloride

Y. X. Liu, X. R. Zhu, X. Sun, W. Yan, J. Xu *
School of Physics and Electronic Engineering, Jiangsu University, Zhenjiang, Jiangsu, 212013, P. R. China

The cocatalyst is crucial in promoting charge separation and surface reaction kinetics in the photocatalytic process. In this study, a novel photocatalyst was prepared via a one-step hydrothermal approach, integrating the commonly used semiconductor material cadmium sulfide with activated carbon (AC), forming a Schottky junction between them. The interfacial C-S bond between CdS and AC serves as an atomic-scale electron transfer pathway, lowering the interfacial charge transfer barrier. The synergistic effect of the Schottky junction and the C-S chemical bond improves the efficiency of e-h pair separation and effectively optimizes charge transfer dynamics. Moreover, the specific surface area of activated carbon (AC) is high, which gives the composite a certain adsorption capacity. Experimental results indicate that when the concentration of TCH is 20 mg/L, the photocatalytic degradation effect of CdS/AC(4:1) was the best. The degradation rate of only 5mg could reach 58.67% in 20 min, far exceeding that of CdS. After 60 minutes, the degradation rate was 77.74%, higher than 60.20% of CdS. This study provides reliable guidance for the design and preparation of low-cost and efficient CdS cocatalysts, and opens up a new general solution and possibility for addressing the environmental pollution resulting from the misuse of antibiotics.

(Received April 22, 2025; Accepted July 23, 2025)

Keywords: CdS, Activated carbon, Degradation, Photocatalysis, Tetracycline hydrochloride

1. Introduction

With the advancement of medical technology, the research and demand for antibiotics are increasing [1, 2]. But antibiotics in the environment pose ecological risks: they are both ecologically toxic and promote the spread of antibiotic-resistant bacteria (ARB) and resistance genes (ARG) [3]. Taking tetracycline hydrochloride (TCH) as an example, as a commonly used antibacterial drug [4], it cannot be fully absorbed by humans and animals. A large amount of it remains in wastewater and soil and returns to the human body through environmental pathways. Long-term intake can lead to microbial disturbance and affect the absorption of B vitamins [5]. Therefore, solving the problem of antibiotic residues in scenarios such as hospital wastewater has become a key environmental challenge [6]. Fortunately, various methods have already been developed to treat antibiotics in wastewater, including electrochemical techniques [7-10], membrane filtration [11], ion exchange [12], biological treatments [13], adsorption [14-16], photocatalysis [17-20], and so forth. Among the aforementioned treatment methods, photocatalysis stands out as a green and environmentally friendly approach due to its efficient and sustainable utilization of sunlight [21-23], and it plays an important role in the degradation of antibiotics [24], pigments, and pesticides [25, 26].

Cadmium sulfide (CdS), a well-known semiconductor material with a narrow bandgap, is widely regarded as an effective photocatalyst due to its strong visible light response [27]. Nevertheless, the slight corrosion of CdS, the swift recombination of electron-hole pairs, and the scarcity of surface catalytic sites constrain the use of pure CdS. The integration of carbon materials as co-catalysts with CdS can effectively suppress sulfide aggregation, enhance structural stability, and facilitate efficient charge carrier separation, thereby significantly improving the photocatalytic

* Corresponding author: xjing@ujs.edu.cn
https://doi.org/10.15251/DJNB.2025.203.843

performance of pristine CdS. Among various reported carbon materials, activated carbon (AC) has emerged as a promising candidate for photocatalytic applications due to its microporous structure and abundant surface functional groups. For instance, Alsaiari developed a photocatalytic composite made from activated carbon derived from biomass and TiO_2. The incorporation of activated carbon notably enhanced the photocatalytic reduction efficiency by effectively segregating the photogenerated electrons and holes, thereby successfully converting Cr (VI) to Cr (III) and degrading methylene blue (MB) dye when exposed to visible light [28]. Faisal et al. developed an innovative ternary mixture comprising semiconductor metal oxide (ZnO-SnO_2) alongside activated carbon (AC). In this configuration, AC serves effectively as an electron acceptor, creating a trap for electrons generated by light, which in turn prolongs carrier recombination and enhances the photocatalytic performance [29]. However, poor interfacial contact acts like a "wall" between the two materials, severely hindering the charge transfer pathway. Recently, Sun et al. have achieved significant progress in successfully fabricating a Schottky junction photocatalyst featuring a P-Ni bond. Within this system, the discrepancy in the Fermi level facilitates the migration of electrons from PCN to NiS through the P-Ni chemical bond. Additionally, the Schottky junction established between the two components impedes electron backflow, thereby boosting the photocatalytic hydrogen - evolution efficiency [30]; Ai et al. successfully synthesized a novel ZnO/In_2S_3 S-type heterojunction composite material through a one-step hydrothermal method, which has S-O chemical bonds and reduces the interfacial charge transfer energy barrier. Electrons migrate from IS to ZO through S-O chemical bonds upon contact, ensuring high reduction ability of photo-generated electrons in IS and high oxidation ability of photo-induced holes in ZO, thereby improving the degradation efficiency and hydrogen production efficiency of tetracycline hydrochloride [31]. These results demonstrate that interfacial chemical bonds can serve as atomic-level carrier transport channels, reducing the electron transfer distance from one material to another. This significantly lowers the interfacial charge transfer energy barrier and enhances the photocatalytic performance.

Herein, a CdS/AC nanoschottky junction with abundant C-S bonds between AC and CdS was constructed by uniformly growing CdS on AC using the hydrothermal method, which is an effective photocatalyst for visible light photocatalytic degradation of TCH. In the intelligent construction of this CdS/AC catalyst, AC and CdS are used as co-catalysts and photo-collecting photocatalysts, respectively. The varying work functions of the two create substantial driving forces for electron movement, directing electrons in the conduction band of CdS to migrate to AC. Notably, the C-S bond formed between CdS and AC serves as a rapid electron transfer pathway at the atomic level, enhancing the charge transfer during photocatalysis. Additionally, the considerable specific surface area of AC imparts a significant adsorption capability to the composite material. Therefore, the catalyst exhibits significantly enhanced photocatalytic performance, with a higher degradation rate and efficiency in TCH compared to pure CdS. Experiments have shown that when the TCH concentration is 20 mg/L, CdS/AC(4:1) exhibits the best photocatalytic degradation performance, with a degradation rate of 58.67% within 20 minutes, much faster than CdS. After 60 minutes, the degradation rate can reach 77.74%, higher than 60.20% of CdS. This work provides a constructive reference for efficient photocatalytic reactions at atomic-level interfaces and Schottky structures.

2. Materials and methods

2.1. Chemicals

Thiourea (CH_4N_2S), cadmium nitrate tetrahydrate ($Cd(NO_3)_2 \cdot 4H_2O$), activated carbon (AC), and sodium hydroxide (NaOH) flakes are directly obtained from Sinopharm Chemical Reagent (Shanghai, China). Tetracycline hydrochloride (TCH) was purchased from Shanghai Macklin Biochemical Technology Co., Ltd. The chemicals used were all of analytical purity, and the water used was laboratory-grade deionized water.

2.2. Preparation of CdS/AC and CdS

CdS/AC is synthesized using a hydrothermal method. Initially, 72.2 mg of activated carbon (AC) is added to 80 mL of deionized water in a beaker and magnetically stirred for one hour. Subsequently, 617 mg of $Cd(NO_3)_2 \cdot 4H_2O$ and 285.6 mg of CH_4N_2S are dissolved into the AC

suspension respectively. Once the components are completely dissolved, adjust the pH to 11 by using a 2 mol·L^{-1} NaOH solution, and then continue for 24 hours. The resulting mixture was then transferred into a Teflon-lined autoclave with a capacity of 100 mL and heated in an oven at 180°C for 12 hours. The collected yellowish-brown powder was rinsed multiple times with deionized water until a neutral pH was achieved, then centrifuged, dried overnight at 80°C in an oven, and finally finely ground. The CdS/AC sample synthesized by this method was named CdS/AC(4:1). Under the same reaction conditions, the mass of AC was altered to 0, 48.1, and 144.4 mg, yielding samples named CdS, CdS/AC(6:1), and CdS/AC(2:1), respectively. To demonstrate the synthesis process, the steps are depicted in Fig.1.

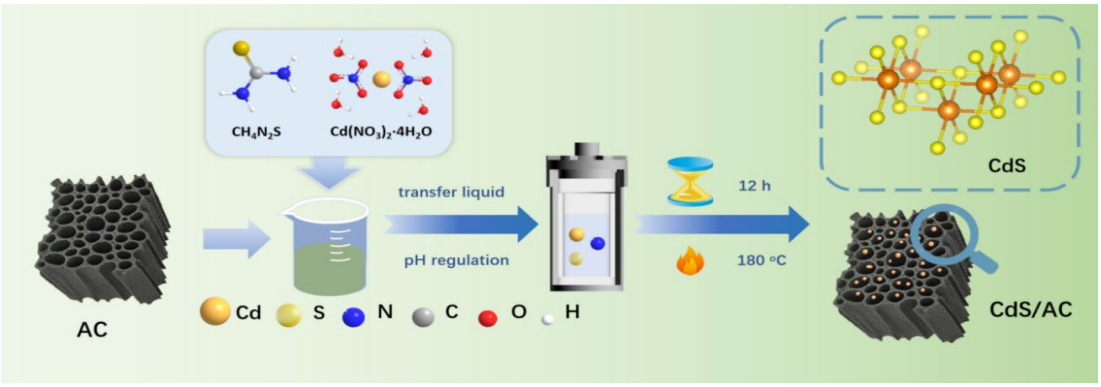

Fig. 1. Illustration of the preparation of CdS/AC.

2.3. Photocatalytic performance

In this study, the degradation performance of the prepared material under visible light was assessed using TCH as the target for degradation. A quantity of 5 mg of the produced photocatalyst was added to 100 mL of a 20 mg L^{-1} TCH solution, followed by 30 minutes of magnetic stirring in the dark to reach adsorption-desorption equilibrium. After that, the solution was uniformly irradiated by a 30 W visible-light lamp (emission wavelength 405 nm) for photodegradation tests. Every 10-minute interval had 3.5 mL of the mixture being drawn out with a syringe, filtered through a water filtration needle, and transferred to a 5 mL plastic centrifuge tube for subsequent analysis. After 60 min of illumination, the absorbance of the reaction mixture at TCH's maximum absorption wavelength (357 nm) was measured by using a UV-visible spectrophotometer. This method was adopted to study the photodegradation capability of different dosed samples under varying time and concentration conditions. The degradation rate of TCH was worked out by using the following formula.

$$\text{Degradation Rate}=[(C_0-C_t)/C_0]*100\%$$

3. Results and discussion

3.1. Structural characterization

The samples were examined through scanning electron microscopy (SEM) to assess their morphologies. As shown in Fig.2a, the AC sample displays a relatively coarse layered structure and has numerous pores on its surface. This feature suggests a large specific surface area, creating optimal conditions for the uniform growth of CdS nanoparticles. As evident from Fig.2b, CdS particles tend to agglomerate and are composed of several small spherical particles, which are not favorable to the photocatalytic reaction. From Fig.2c, it can be observed that CdS nanoparticles grow

uniformly and densely on the AC surface, tightly integrated with it, and the agglomeration of CdS nanoparticles is correspondingly reduced. CdS/AC (2:1) and CdS/AC (6:1) have similar structures to CdS/AC (4:1), but with different proportions (Fig.S1). This leads to a greater exposure of active sites within the composite material, creating optimal conditions for the degradation process driven by photocatalysis [32].

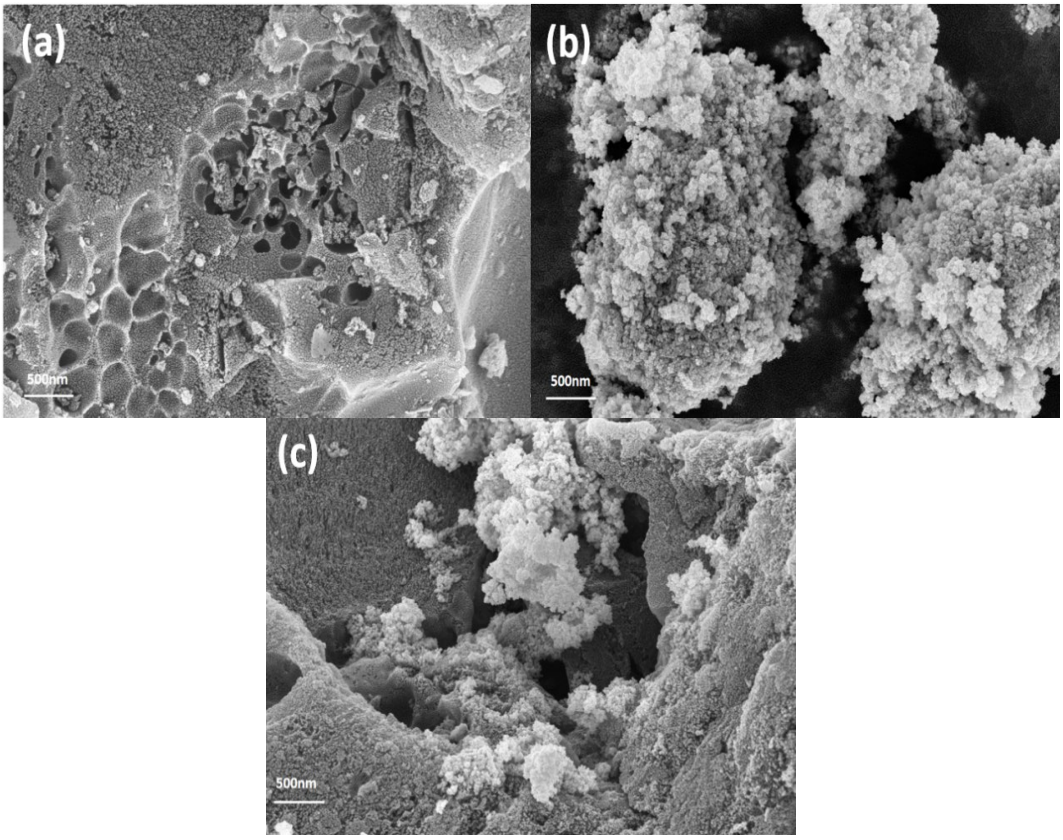

Fig. 2. SEM images of AC (a), CdS (b), and CdS/AC(4:1) (c).

An XRD analysis was conducted with the aim of performing a more detailed analysis of the samples' crystal structure. In Fig.3a, a distinctive peak is shown in AC at 26.6°, which is associated with the (002) plane of graphitic materials (PDF#04-007-8496). CdS shows characteristic diffraction peaks at 24.9°, 26.5°, 28.3°, 30.3°, 43.9°, 47.9°, and 52.0°, consistent with the hexagonal phase of CdS (PDF#97-062-0308). In Fig. 3 b, the three composites with different ratios exhibit typical characteristic diffraction peaks of CdS and AC. However, the characteristic peaks of the composites are weaker than those of CdS alone, indicating that CdS has been successfully anchored onto activated carbon via the hydrothermal method. Since AC is amorphous carbon, the broad peak of AC only has a weakly graphitized microcrystalline structure, which is not observed in the composites [33]. Moreover, the light absorption properties of CdS and the CdS/AC composite were evaluated through UV-Vis NIR spectroscopy. As illustrated in Fig.3c, the CdS/AC composites demonstrate a greater capacity for visible light absorption in comparison to pure CdS, with the extent of enhancement varying based on the ratio of AC. This enhancement can largely be credited to the incorporation of AC, which modifies the color of the material and consequently expands the absorption spectrum. Consequently, these composite materials show markedly improved absorption within the visible light range when compared to pure CdS, thereby boosting their photothermal efficiency and improving sunlight utilization [34, 35]. The band gap widths for the samples, calculated using the Kubelka-Munk equation, are presented in Fig.3d. CdS has an approximate band gap of 2.25 eV, while CdS/AC(4:1) shows a value of 2.20 eV. This reflects the interaction or

interface contact strength between the co-catalyst AC and CdS, enabling the CdS/AC composite material to exhibit better visible light harvesting capability and enhanced charge separation and transfer efficiency [36-38].

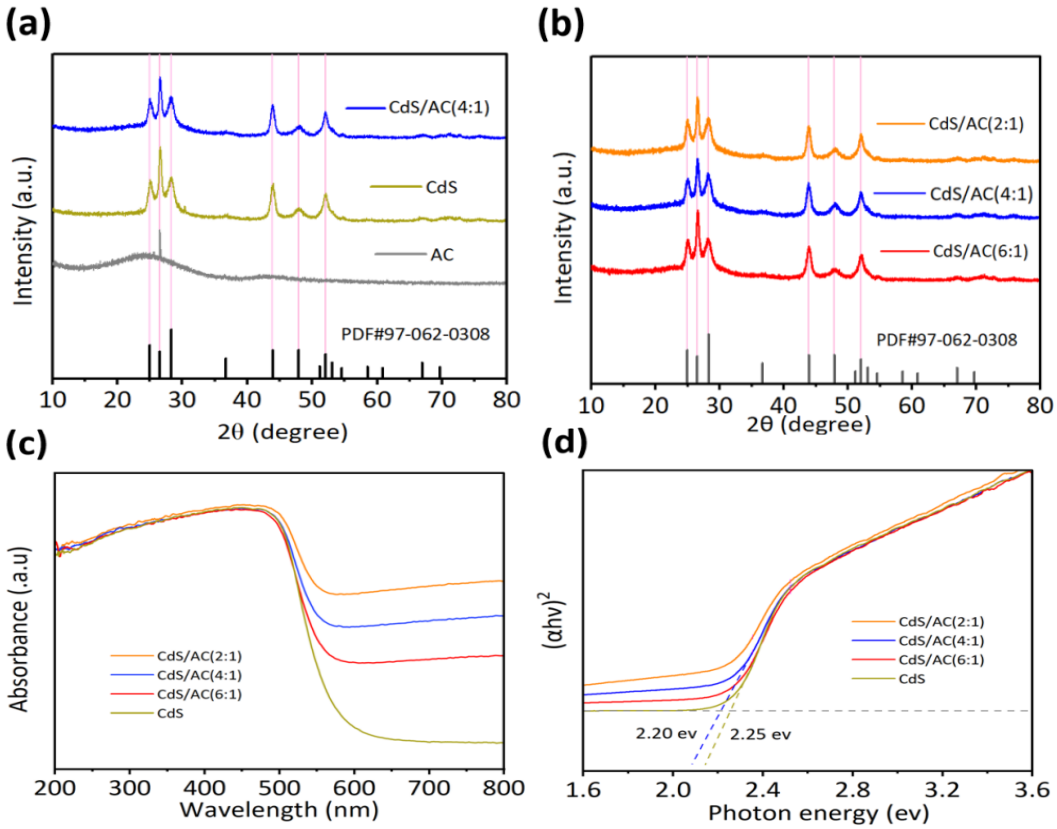

Fig. 3. XRD patterns (a, b) and UV-Vis NIR (c, d) of CdS, AC and CdS/AC.

3.2. Charge carrier dynamics behavior

XPS was employed to assess the elemental composition and chemical states of CdS and the CdS/AC(4:1) composite. The results shown in Fig.4a indicated characteristic peaks for three elements: C 1s, S 2p, and Cd 3d. In the C 1s spectrum (Fig.4b), for the CdS sample, a peak at 284.8 eV is associated with the C-C bond, which is typically considered an indication of carbon in the sample. Additionally, the peaks at 288.29 eV as well as 286.28 eV are related to the C=O and C-O bonds, respectively. For CdS/AC(4:1), the binding energies of these three bonds were determined to be lower. As changes in binding energy can directly reflect variations in electron density[39], it can be inferred that AC gained electrons. The Cd 3d XPS spectrum (Fig.4c) shows two symmetric peak pairs for CdS at 404.75 eV as well as 411.46 eV, which correspond to Cd $3d_{5/2}$ and Cd $3d_{3/2}$. These values are consistent with the characteristic binding energy of Cd in the +2 valence state in cadmium sulfide. Similarly, the S 2p XPS spectrum (Fig.4d) shows the S 2p peaks for CdS at 161.15 eV and 162.38 eV, corresponding to the electronic states of $S2p_{3/2}$ and S $2p_{1/2}$, and in line with the binding energy characteristic of S in the -2 valence state in cadmium sulfide. Notably, a new peak at 168.57 eV exists in the CdS/AC (4:1) sample, corresponding to the C-S bond [40, 41]. This bond acts as an atomic-level interface for electron transfer between CdS and AC, further confirming the growth of CdS and improving electron separation and transfer. Moreover, the binding energies related to Cd 3d and S 2p in the CdS/AC (4:1) composite exhibit a significant shift to higher energy levels, indicating an electron loss. Consequently, the experimental data imply that electrons are transferred from CdS to AC, while C-S chemical bonds serve as electron transport channels at the atomic level.

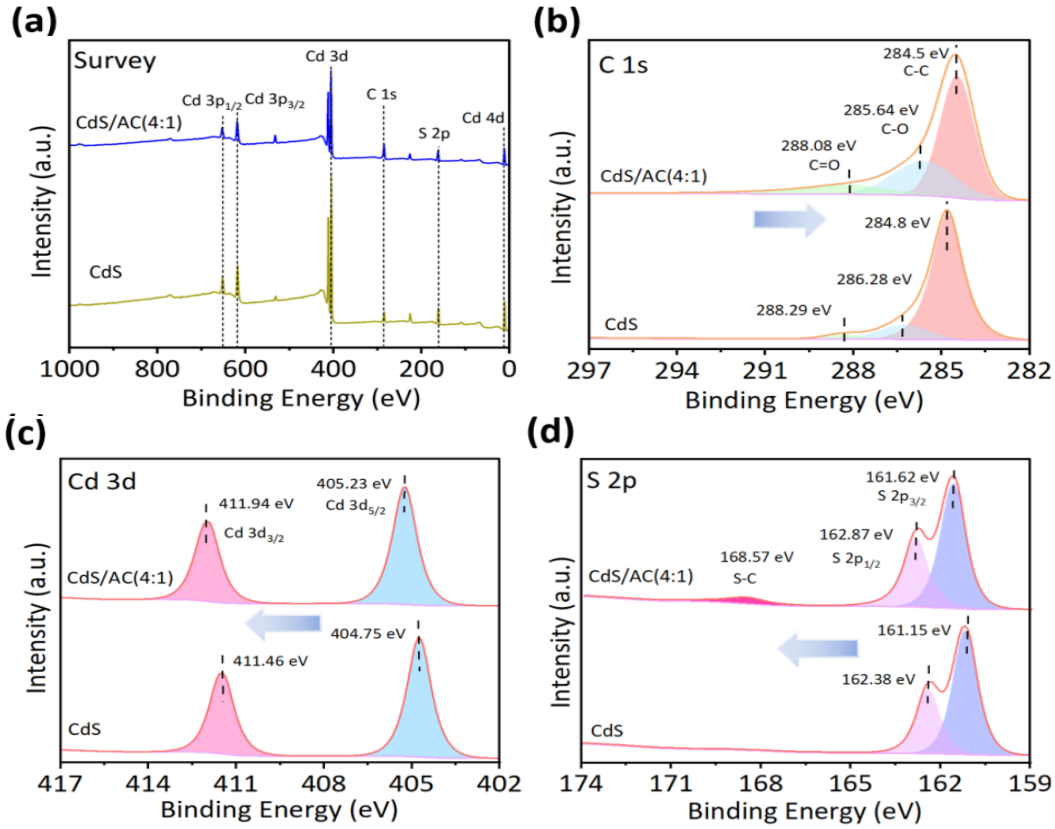

Fig. 4. XPS survey spectra of CdS/AC(4:1) and CdS (a).
High-resolution XPS spectra of C 1s (b), Cd 3d (c), and S 2p (d).

A crucial factor influencing catalytic efficiency is the recombination rate of carriers. A decrease in the recombination rate is associated with improved catalytic performance. As illustrated in Fig.5a, both CdS and CdS/AC(4:1) present similar emission peaks, however, the fluorescence intensity observed for CdS/AC(4:1) is markedly lower compared to that of pure CdS. The reduced intensity of fluorescence indicates a decline in the rate of recombination for electron-hole pairs generated by illumination. Consequently, the incorporation of AC promotes electron transfer, which leads to a lower recombination rate of carriers within CdS. The results from fluorescence lifetime detection (Fig.5b) further support this observation. After double exponential fitting, the experimental data show that the average lifetime (τave) of CdS is 3.75 ns, whereas for CdS/AC(4:1), τave increases to 4.70 ns, reflecting a 25.3% increase. The extended carrier lifetime allows more electrons and holes to participate in redox reactions. Additionally, carriers with longer lifetimes can migrate within or on the surface of the catalyst to regions more favorable for the reaction, increasing the likelihood of interactions with the target degradation product. The transient photocurrent responses of CdS and the CdS/AC(4:1) composite were recorded in Fig.5c. By analyzing the graphs, the differences are compared in photocurrent generation between these two samples are compared. Following exposure to visible light, there was a rapid generation of photocurrent. Once the light was switched off, the photocurrent swiftly returned to its original level. Upon completion of several cycles, the photocurrent for these materials began to level off. Importantly, the photocurrent observed in the CdS/AC(4:1) composite showed a notable increase in comparison to that of CdS. This illustrates that the separation of electrons and holes is taking place more effectively, leading to a longer lifetime of the photo-generated carriers in CdS/AC(4:1), which aligns with the conclusions derived from the PL results [42]. Additionally, EIS analysis was conducted to confirm that CdS/AC(4:1) exhibits a more rapid electron transfer rate. Illustrated in Fig.5d, the semicircular radius for CdS/AC(4:1) is considerably less than that for pure CdS. These results reveal that the resistance to interfacial charge carrier transfer in the CdS/AC(4:1) composite is lower than that in

pure CdS. The composite demonstrates diminished interfacial resistance, facilitating the prompt and efficient separation of photogenerated charge carriers. This occurrence can be explained by the Schottky junction established at the interface, which promotes directional electron transfer due to the driving force created by the interfacial energy differences. Furthermore, the C-S bonds present at the interface serve as effective channels for electron transport, significantly improving the dynamics of charge carrier migration [43, 44].

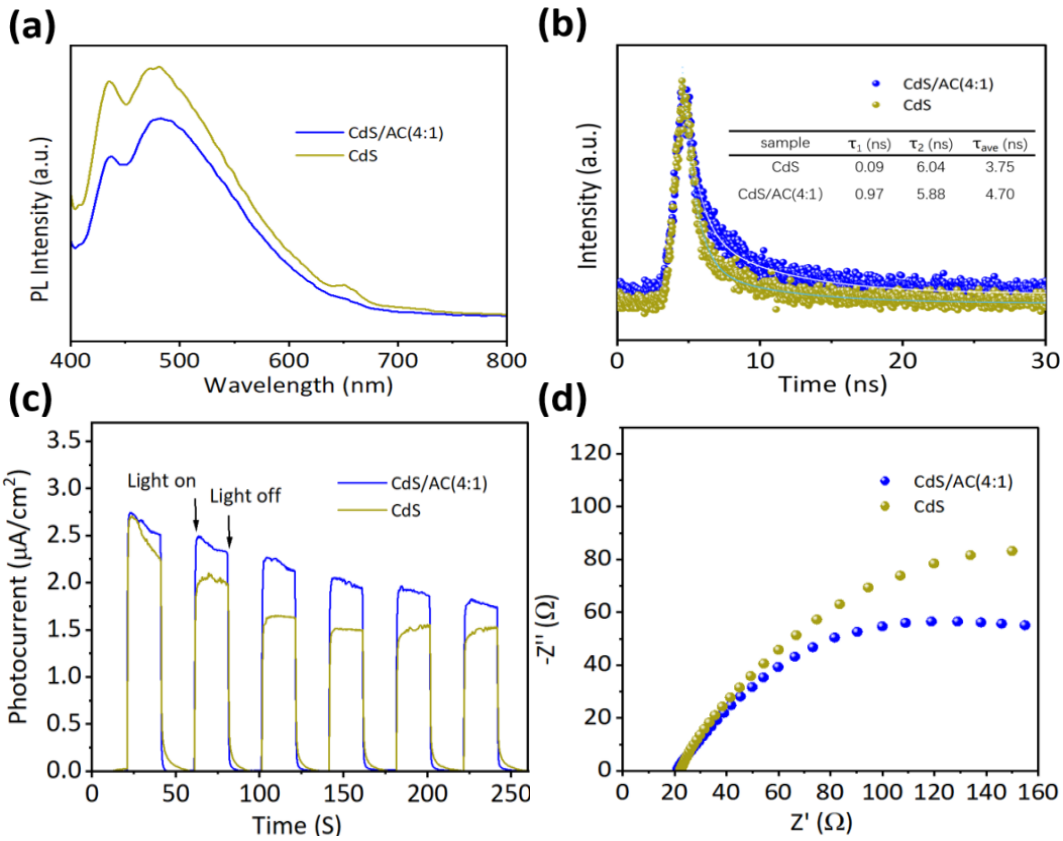

Fig. 5. Steady-state photo-luminescence (PL) spectra (a). Time-resolved PL spectra of CdS/AC(4:1) and CdS (b). Photocurrent response (c) and Nyquist plots (d) of the CdS and CdS/AC(4:1) samples.

3.3. Photocatalytic performance evaluation

Fig.6 illustrates the photodegradation capability of the samples. As evident from Fig.6a, both pure AC and pure CdS exhibit unsatisfactory degradation effects on TCH. The introduction of AC significantly enhances the degradation efficiency of CdS on TCH. From Fig.6b, it can be observed that samples with varying proportions of AC incorporation show improvements over pure CdS and that, among various composite samples with different proportions, CdS/AC(4:1) has the best degradation ability, significantly outperforming other samples. This is because when the amount of AC is small, the adsorption and charge transfer effect of CdS on AC is not obvious. When AC is excessive, the active component in the composite catalyst is insufficient, which leads to the degradation efficiency. Adapting the photocatalytic degradation process of TCH to align with a pseudo-first-order kinetic model enabled us to calculate the reaction rate constants for various samples, allowing for a quantitative assessment of their degradation rates. As illustrated in Fig.6c, the CdS/AC(4:1) sample displayed the highest degradation rate constant, which is 1.56 times higher than that of the CdS. Fig.6d reflects the degradation rate curves of different samples from the dark reaction to 60 minutes of light exposure. The adsorption capacity of the sample during the dark reaction process shows a positive correlation with the carbon doping content of the sample. AC has little effect on its adsorption due to light exposure, resulting in no significant change in its overall

rate. The degradation rate of other samples increases and then decreases after exposure to light. Within 60 minutes, CdS/AC (4:1) achieved a TCH degradation rate of 77.74%, which is higher than the 60.20% degradation rate of CdS. Additionally, it had a significant advantage in degradation speed. At 20 minutes, the degradation rate of CdS/AC(4:1) was almost three times that of CdS, which was equivalent to the degradation rate of CdS at 60 minutes. Under other experimental conditions, CdS/AC(4:1) also demonstrated significant advantages (Fig.S2,3). The mechanical stirring degradation diagram (Fig.S4) demonstrates the degradation performance of CdS/AC (4:1), which is superior to simply mixing CdS with AC in the same proportion. This confirms the significant contribution of the Schottky junction and electron transfer pathway formed between the two materials to the degradation process. Simultaneously, Fig.S5 shows its cyclic degradation effect, indicating the stability of its photocatalytic degradation activity, which means that it can be reused multiple times with practicality.

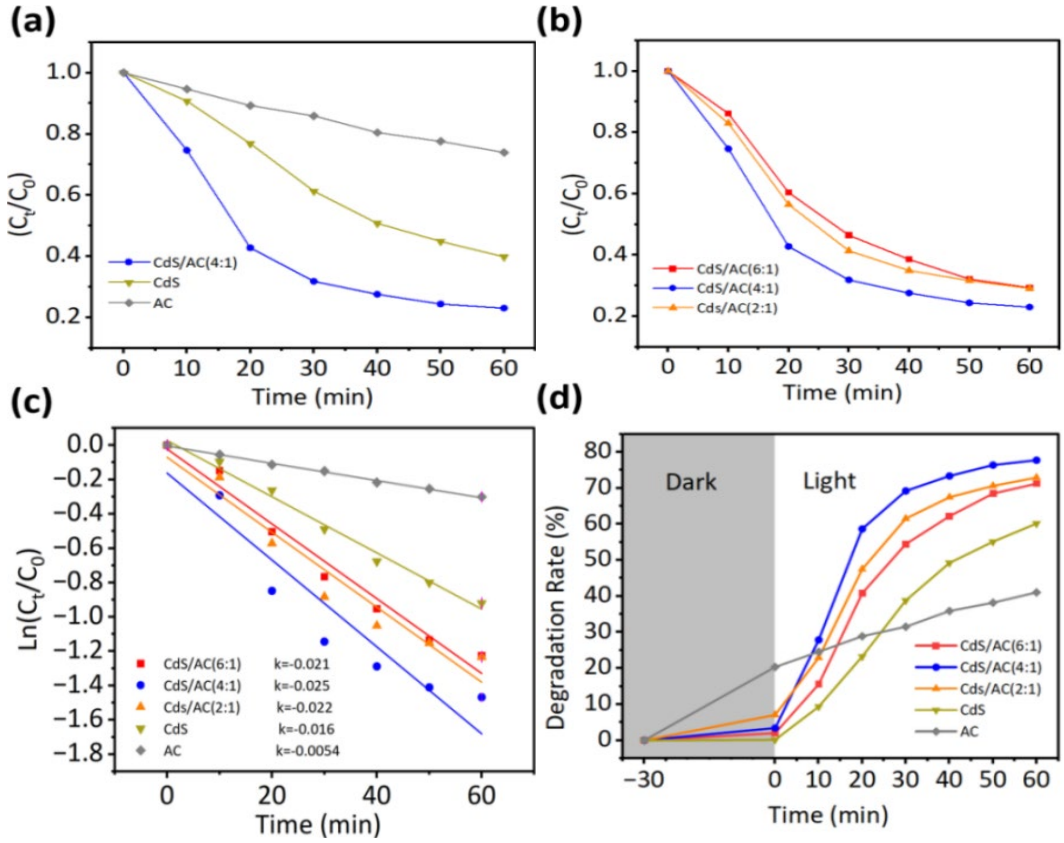

Fig. 6. Change in the proportion of degradation products (a, b), first-order pseudo-kinetic fitting curve (c), and photo-degradation rate (d) of a 5 mg sample at a TCH concentration of 20 mg·L^{-1}.

3.4. The adsorption effect of AC

Fig.7 presents the results of the BET test for both AC and CdS/AC (4:1). As illustrated in Fig.7a,the isotherms of two samples are classified as type IV isotherms accompanied by hysteresis loops, indicating their mesoporous nature. Additionally, the adsorption-desorption curves show significant hysteresis, manifesting as H3-type hysteresis loops [45, 46]. This indicates that AC does not have a distinct saturated adsorption platform, suggesting its irregular pore structure, which includes slit-like structures, wedge-like structures, etc. Experimental measurements reveal that the specific surface area of AC is 1269.31 m²/g, while the surface area of CdS/AC (4:1) after AC composite reaches 262.5182 m²/g. The pore size distribution diagram (Fig.7b) indicates that the material primarily exhibits a mesoporous structure. The total pore volumes of AC and CdS/AC (4:1) are 0.780419 cm³/g and 0.416198 cm³/g. The pore size distribution of CdS/AC (4:1) matches that of

AC. Therefore, it is the characteristics of AC enable the CdS/AC composite to have stronger adsorption capacity, stability, and a higher probability of contact with reactants compared to CdS.

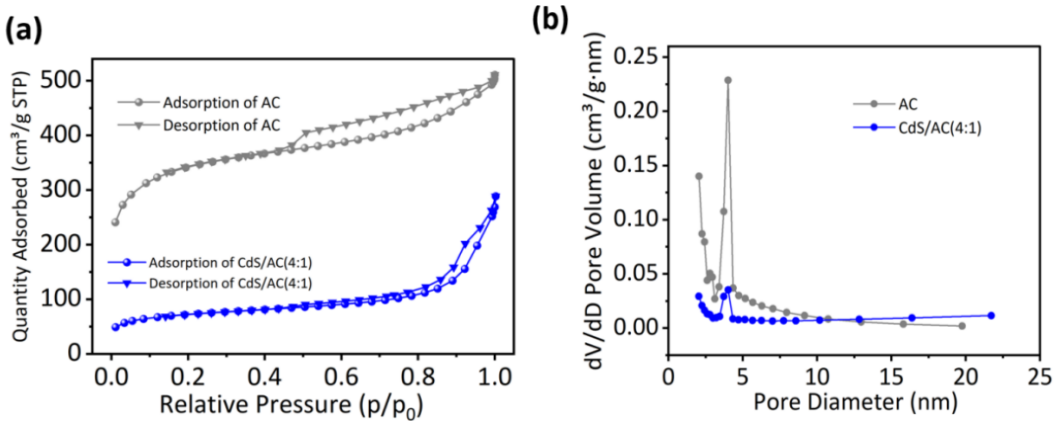

Fig. 7. N2 adsorption-desorption isotherms (a), pore size distributions (b) of AC and CdS/AC(4:1).

3.5. Photocatalytic mechanism

XPS analysis revealed changes in the binding energy of the CdS/AC composite material. The disparity in work functions or Fermi levels between CdS and AC constitutes the fundamental internal driving force underlying the charge transfer process within the CdS/AC composite system, thereby resulting in the formation of the schottky junction structure. As shown in Fig.8, AC exhibits a relatively large work function value and a lower Fermi level, designated as E_{f2}, whereas CdS is characterized by a smaller work function magnitude and a higher Fermi level, denoted as E_{f1}. The divergence of the Fermi level makes the electrons of CdS diffuse to AC through the C-S chemical bond until the Fermi level positions of CdS and AC are equal when they are in close contact, forming a Schottky junction [47, 48]. Constructing schottky junctions and designing hybrid composites are widely recognized strategies for improving photocatalytic efficiency [49, 50]. When exposed to light, CdS produces photoelectrons (e) within the conduction band and photogenerated holes (h+) in the valence band. The Schottky junction created by the interaction of CdS and AC establishes an energy band that curves upward, effectively impeding the reverse flow of electrons and significantly improving the efficiency of separation and transfer of photogenerated carriers. Given its metallic characteristics, AC functions as an active site that promptly transfers electrons to its surface, thus raising the concentration of electrons on the material's surface [51, 52]. The migration of these charge carriers suppresses their recombination of in CdS, thereby prolonging the carrier lifetime and significantly improving the photocatalytic performance. As a result, vacancies build up in the valence band of CdS, whereas electrons gather in AC. Following this, the electrons present in AC interact with O_2, converting it into superoxide radicals ($\cdot O_2^-$), while the holes facilitate the reduction of H_2O, leading to the production of hydroxyl radicals ($\cdot OH$) [53]. These two highly oxidizing active species serve as the primary substances for the photodegradation of TCH under light, oxidizing and decomposing it into small molecules. Meanwhile, the adsorption properties of AC itself also play a synergistic role, with its surface rich in pore structures adsorbing part of the TCH. Additionally, the surface functional groups enhance adsorption sites, promoting chemical bonding and chemisorption with TCH [54]. This process enriches pollutants while optimizing the reaction interface, ultimately achieving efficient degradation of TCH through the synergistic effects of photocatalytic oxidation and adsorption.

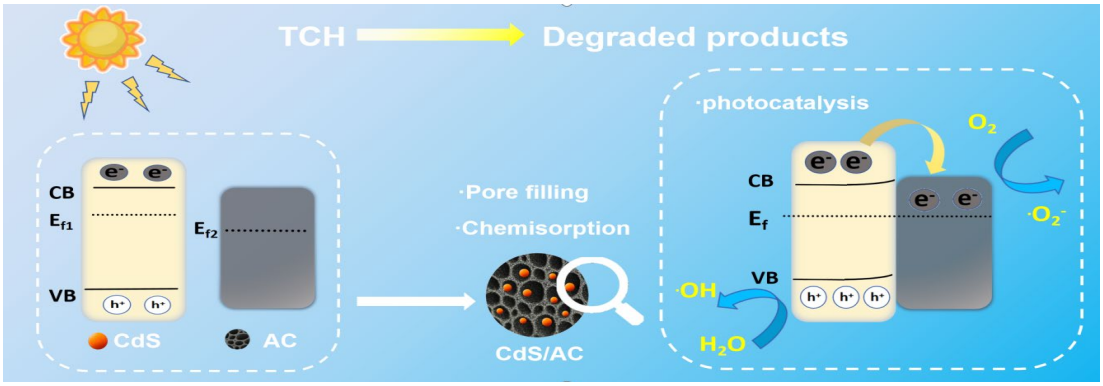

Fig. 8. Mechanisms of degradation of TCH by CdS/AC(4:1) under light irradiation.

4. Conclusion

In this study, we successfully synthesize an innovative CdS/AC Schottky junction by incorporating available AC into the hydrothermal synthesis of CdS. The CdS/AC with the optimal composition ratio exhibits excellent photocatalytic performance, enabling it to achieve satisfactory degradation of TCH under visible light. The experimental results proved the fact that, under specific conditions, the degradation rate of CdS/AC (4:1) is significantly improved compared to AC and CdS, with a degradation rate of 77.74% in 60 minutes. The characterization results confirm that AC, as an economical cocatalyst, promotes electron transfer by forming C-S interface chemical bonds with CdS, which act as electronic channels and enhance charge carrier transfer kinetics. Additionally, AC creates upward band bending, preventing electrons from returning to CdS, enhancing the efficiency of electron transfer, and extending the lifespan of charge carriers. The extremely high specific surface area of AC also endows CdS/AC with a certain adsorption capacity to assist in the degradation of pollutants. Therefore, CdS/AC has a good development space in the field of photocatalytic degradation of environmental antibiotics, and the synthesis method is universal and simple.

Supporting information

Characterizations, XRD patterns of the samples were recorded by using a Malvern Panalytical Empyrean X-raydiffractometer. Surface morphology was observed using a Zeiss Sigma 300 field emission scanning electron microscope (SEM). XPS measurements were conducted on a Thermo Fisher Nexsa X-ray photoelectron spectrometer instrument. DRS of the samples were acquired using a Shimadzu 3600-plus ultraviolet-visible near-infrared spectrometer. PL spectra were recorded on an Edinburgh FLS-1000 steady-state/transient fluorescence spectrometer. Photoelectrochemical properties, including transient photocurrent responses and EIS, were measured on a Corrtest CS310H electrochemical workstation in a standard three-electrode system. The pore size distribution and specific surface area of the samples (BET) were measured using the Micromeritics ASAP2460 analyzer.

Acknowledgments

This work was supported by the Innovation and Entrepreneurship Training Program for University Students in Jiangsu Province (Project No.202410299087Z)

References

[1] L. Jiang, D.L. Wei, K. Zeng, J. Shao, F. Zhu, D.L. Du, Food Analytical Methods 11, 2066-2075 (2018); https://doi.org/10.1007/s12161-018-1185-2
[2] Y. Dai, W.G. Peng, Y. Ji, J. Wei, J.H. Che, Y.Q. Huang, W.H. Huang, W.M. Yang, W.Z. Xu, Journal of Food Science 89, 8022-8035 (2024); https://doi.org/10.1111/1750-3841.17398
[3] H. Xue, L. Deng, D. Kang, Y. Zhao, X. Zhang, Y. Liu, H. Chen, H.H. Ngo, W. Guo, Journal of Environmental Chemical Engineering 12, 114275 (2024); https://doi.org/10.1016/j.jece.2024.114275
[4] R. Han, Y. Song, J. Duan, S. Ai, Colloids and Surfaces A: Physicochemical and Engineering Aspects 702, 134974 (2024); https://doi.org/10.1016/j.colsurfa.2024.134974
[5] F. Zhang, J. Wang, Y. Tian, C. Liu, S. Zhang, L. Cao, Y. Zhou, S. Zhang, Environmental Pollution 330, 121681 (2023); https://doi.org/10.1016/j.envpol.2023.121681
[6] J. Tell, D.J. Caldwell, A. Häner, J. Hellstern, B. Hoeger, R. Journel, F. Mastrocco, J.J. Ryan, J. Snape, J.O. Straub, J. Vestel, 15, 312-319 (2019); https://doi.org/10.1002/ieam.4141
[7] H. Pourzamani, N. Mengelizadeh, H. Mohammadi, N. Niknam, B. Neamati, R. Rahimi, Desalination and Water Treatment 113, 307-318 (2018); https://doi.org/10.5004/dwt.2018.22275
[8] X. Wang, Y. Pan, X. Wang, Y. Guo, C. Ni, J. Wu, C. Hao, Industrial Crops and Products 189, 115863 (2022); https://doi.org/10.1016/j.indcrop.2022.115863
[9] L. Luo, X. Liu, S. Ma, L. Li, T. You, Food Chemistry 322, 126778 (2020); https://doi.org/10.1016/j.foodchem.2020.126778
[10] S. Liu, S. Meng, M. Wang, W. Li, N. Dong, D. Liu, Y. Li, T. You, Food Chemistry 410, 135450 (2023); https://doi.org/10.1016/j.foodchem.2023.135450
[11] A. Arminini Neto, E.F.D. Januário, T.B. Vidovix, N.d.C.L. Beluci, R. Bergamasco, A.M.S. Vieira, Chemical Engineering and Processing - Process Intensification 202, 109837 (2024); https://doi.org/10.1016/j.cep.2024.109837
[12] G. Jalloul, N. Hijazi, C. Boyadjian, H. Awala, A.B. Albadarin, M.N. Ahmad, Heliyon 10, (2024); https://doi.org/10.1016/j.heliyon.2024.e31854
[13] A.S. Oberoi, Y. Jia, H. Zhang, S.K. Khanal, H. Lu, Environmental Science & Technology 53, 7234-7264 (2019); https://doi.org/10.1021/acs.est.9b01131
[14] M. He, L. Zhao, H. Hu, L. Yao, Y. Guo, C. Hou, S. Gao, R. Li, Environmental Research 263, 120193 (2024); https://doi.org/10.1016/j.envres.2024.120193
[15] H. Liu, P. Li, F. Qiu, T. Zhang, J. Xu, Food and Bioproducts Processing 123, 177-187 (2020); https://doi.org/10.1016/j.fbp.2020.06.018
[16] J. Yuan, Y. Zhu, J. Wang, L. Gan, M. He, T. Zhang, P. Li, F. Qiu, Food and Bioproducts Processing 126, 293-304 (2021); https://doi.org/10.1016/j.fbp.2021.01.004
[17] B. Ma, Y. Zha, H. Shi, Y. Qin, M. Zhao, J. Li, S. Wang, B. Yan, B. Zhao, Y. Ma, H. Xie, Separation and Purification Technology 354, 129086 (2025); https://doi.org/10.1016/j.seppur.2024.129086
[18] J. Xu, W.Y. Cheng, X.B. Liang, R.Y. Wang, Y.C. Wei, H.X. Lao, M. Zhou, W.K. Wang, L.L. Wang, Q.Q. Liu, Journal of Alloys and Compounds 1003, (2024); https://doi.org/10.1016/j.jallcom.2024.175610
[19] J. Xu, X. Zhang, W. Yan, T. Xie, Y. Chen, Y. Wei, Inorganic Chemistry 63, 4279-4287 (2024); https://doi.org/10.1021/acs.inorgchem.3c04408
[20] Y. Chao, J. Pang, Y. Bai, P. Wu, J. Luo, J. He, Y. Jin, X. Li, J. Xiong, H. Li, W. Zhu, Food Chemistry 320, 126666 (2020); https://doi.org/10.1016/j.foodchem.2020.126666
[21] A. Chakravorty, S. Roy, Sustainable Chemistry for the Environment 8, 100155 (2024); https://doi.org/10.1016/j.scenv.2024.100155
[22] J.K. Liang, H.X. Li, L. Chen, M.N. Ren, O.A. Fakayode, J.Y. Han, C.S. Zhou, Industrial Crops and Products 193, (2023); https://doi.org/10.1016/j.indcrop.2022.116214
[23] L. Shen, X. Zhou, C. Zhang, H. Yin, A. Wang, C. Wang, 43, e12931 (2019); https://doi.org/10.1111/jfbc.12931
[24] B. Wang, N.E. Mahoney, Z. Pan, R. Khir, B. Wu, H. Ma, L. Zhao, Food Control 59, 461-467 (2016); https://doi.org/10.1016/j.foodcont.2015.06.030

[25] P.Y. Wang, H.H. Li, M.M. Hassan, Z.M. Guo, Z.Z. Zhang, Q.S. Chen, Journal of Agricultural and Food Chemistry 67, 4071-4079 (2019); https://doi.org/10.1021/acs.jafc.8b07201
[26] X. Du, W. Du, J. Sun, D. Jiang, Food Chemistry 385, 132731 (2022); https://doi.org/10.1016/j.foodchem.2022.132731
[27] T. Wang, Z. Zeng, J. Yang, Z. Pan, X. Zheng, Y. Guo, T. Huang, Colloid and Interface Science Communications 51, 100674 (2022); https://doi.org/10.1016/j.colcom.2022.100674
[28] M. Alsaiari, Arabian Journal of Chemistry 14, 103258 (2021); https://doi.org/10.1016/j.arabjc.2021.103258
[29] M. Faisal, M. Alsaiari, M.A. Rashed, F.A. Harraz, Journal of the Taiwan Institute of Chemical Engineers 120, 313-324 (2021); https://doi.org/10.1016/j.jtice.2021.03.015
[30] D. Sun, T. Zhou, G. Che, C. Liu, Applied Surface Science 578, 152004 (2022); https://doi.org/10.1016/j.apsusc.2021.152004
[31] Y. Ai, J. Hu, X. Xiong, S.A.C. Carabineiro, Y. Li, N. Sirotkin, A. Agafonov, K. Lv, Applied Catalysis B: Environment and Energy 353, 124098 (2024); https://doi.org/10.1016/j.apcatb.2024.124098
[32] S. Shan, Z. Lv, H. Wu, Materials Science and Engineering: B 303, 117272 (2024); https://doi.org/10.1016/j.mseb.2024.117272
[33] H. Li, Y. Dai, X. Li, Z. Shao, Colloids and Surfaces A: Physicochemical and Engineering Aspects 629, 127486 (2021); https://doi.org/10.1016/j.colsurfa.2021.127486
[34] S. Tu, H. Huang, T. Zhang, Y. Zhang, Applied Catalysis B: Environmental 219, 550-562 (2017); https://doi.org/10.1016/j.apcatb.2017.08.001
[35] Y. Liu, X. Dai, J. Li, S. Cheng, J. Zhang, Y. Ma, RSC Advances 14, 478-491 (2024); https://doi.org/10.1039/d3ra06910a
[36] H. Jiang, Z. Hu, Y. Ouyang, X. Ji, X. Hu, T. Li, K. Ouyang, P. Wang, H. Wang, X. Hu, Separation and Purification Technology 326, 124842 (2023); https://doi.org/10.1016/j.seppur.2023.124842
[37] M. Jawad, A. Ur Rahman, S. Hussain Mirza, S. Azam, M.E. Khalifa, S.M. El-Bahy, Chemical Physics 585, 112367 (2024); https://doi.org/10.1016/j.chemphys.2024.112367
[38] N. Yang, J. Zhang, L. Zuo, X. Zeng, R. Cao, Journal of Alloys and Compounds 1021, 179548 (2025); https://doi.org/10.1016/j.jallcom.2025.179548
[39] L. Wang, B. Zhu, B. Cheng, J. Zhang, L. Zhang, J. Yu, Chinese Journal of Catalysis 42, 1648-1658 (2021); https://doi.org/10.1016/S1872-2067(21)63805-6
[40] Z. Fan, X. Guo, Z. Jin, X. Li, Y. Li, Langmuir 38, 3244-3256 (2022); https://doi.org/10.1021/acs.langmuir.1c03379
[41] H.-B. Huang, N. Zhang, K. Yu, Y.-Q. Zhang, H.-L. Cao, J. Lü, R. Cao, ACS Sustainable Chemistry & Engineering 7, 16835-16842 (2019); https://doi.org/10.1021/acssuschemeng.9b04395
[42] L. Zhihua, Z. Xue, H. Xiaowei, Z. Xiaobo, S. Jiyong, X. Yiwei, H. Xuetao, S. Yue, Z. Xiaodong, Food Chemistry 335, 127646 (2021); https://doi.org/10.1016/j.foodchem.2020.127646
[43] H.-B. Huang, Y. Wang, W.-B. Jiao, F.-Y. Cai, M. Shen, S.-G. Zhou, H.-L. Cao, J. Lü, R. Cao, ACS Sustainable Chemistry & Engineering 6, 7871-7879 (2018); https://doi.org/10.1021/acssuschemeng.8b01021
[44] X.. Bi, L. Li, L. Luo, X. Liu, J. Li, T. You, Food Chemistry 385, 132657 (2022); https://doi.org/10.1016/j.foodchem.2022.132657
[45] E.-J. Lee, J.-W. Lee, Bioresource Technology 407, 131124 (2024); https://doi.org/10.1016/j.biortech.2024.131124
[46] M. Javed, H. Huang, Y. Ma, F.-e. Ettoumi, L. Wang, Y. Xu, H.R. El-Seedi, Q. Ru, Z. Luo, Food Chemistry 438, 137948 (2024); https://doi.org/10.1016/j.foodchem.2023.137948
[47] M. Xie, T. Li, X. Zhang, K. Wan, W. Yan, Y. Wei, J. Xu, Journal of Environmental Chemical Engineering 12, 114932 (2024); https://doi.org/10.1016/j.jece.2024.114932
[48] J. Xu, X. Zhang, X. Chen, W. Yan, T. Xie, Y. Chen, Y. Wei, Inorganic Chemistry 63, 17937-17945 (2024); https://doi.org/10.1021/acs.inorgchem.4c03268
[49] L. El Gaini, Desalination and Water Treatment 320, 100798 (2024); https://doi.org/10.1016/j.dwt.2024.100798

[50] P. Jiang, L. Zhou, Y. Han, W. Fu, S. Su, M. Zeng, Journal of Environmental Chemical Engineering 12, 112914 (2024); https://doi.org/10.1016/j.jece.2024.112914
[51] W. Yan, Y. Xu, S. Hao, Z. He, L. Wang, Q. Wei, J. Xu, H. Tang, Inorganic Chemistry 61, 4725-4734 (2022); https://doi.org/10.1021/acs.inorgchem.2c00045
[52] J. Xu, S. Zhu, H. Zhou, M. Hou, K. Wan, X. Zhang, W. Yan, Y. Wei, Y. Chen, 14, 356 (2024); https://doi.org/10.3390/catal14060356
[53] W. Ma, S. Du, S. Suo, Y. Li, J. Guo, Y. Wang, Z. Han, C. Chen, J. Fang, S. Zhang, H. Xu, P. Fang, Surfaces and Interfaces 54, 105240 (2024); https://doi.org/10.1016/j.surfin.2024.105240
[54] J. Hu, B. Mi, L. Chen, Y. Yuan, J. Zhang, F. Wu, International Journal of Biological Macromolecules 276, 134156 (2024); https://doi.org/10.1016/j.ijbiomac.2024.134156

Supporting information

CdS/activated carbon composite for the photocatalysis degradation of tetracycline hydrochloride

Y. X. Liu, X. R. Zhu, X. Sun, W. Yan, J. Xu *
School of Physics and Electronic Engineering, Jiangsu University, Zhenjiang, Jiangsu,212013, P. R. China

*Corresponding author: J. Xu (xjing@ujs.edu.cn)

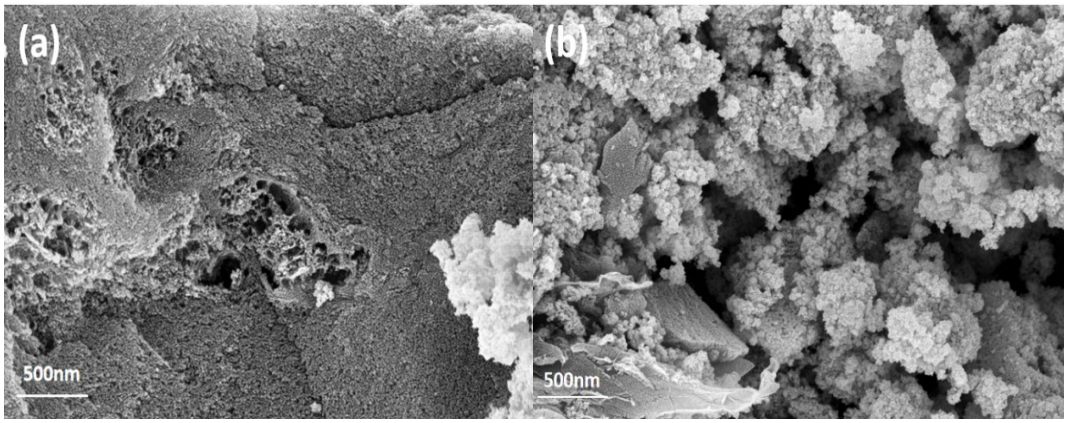

Fig.S1.SEM images of CdS/AC(2:1) (a), CdS/AC(6:1) (b).

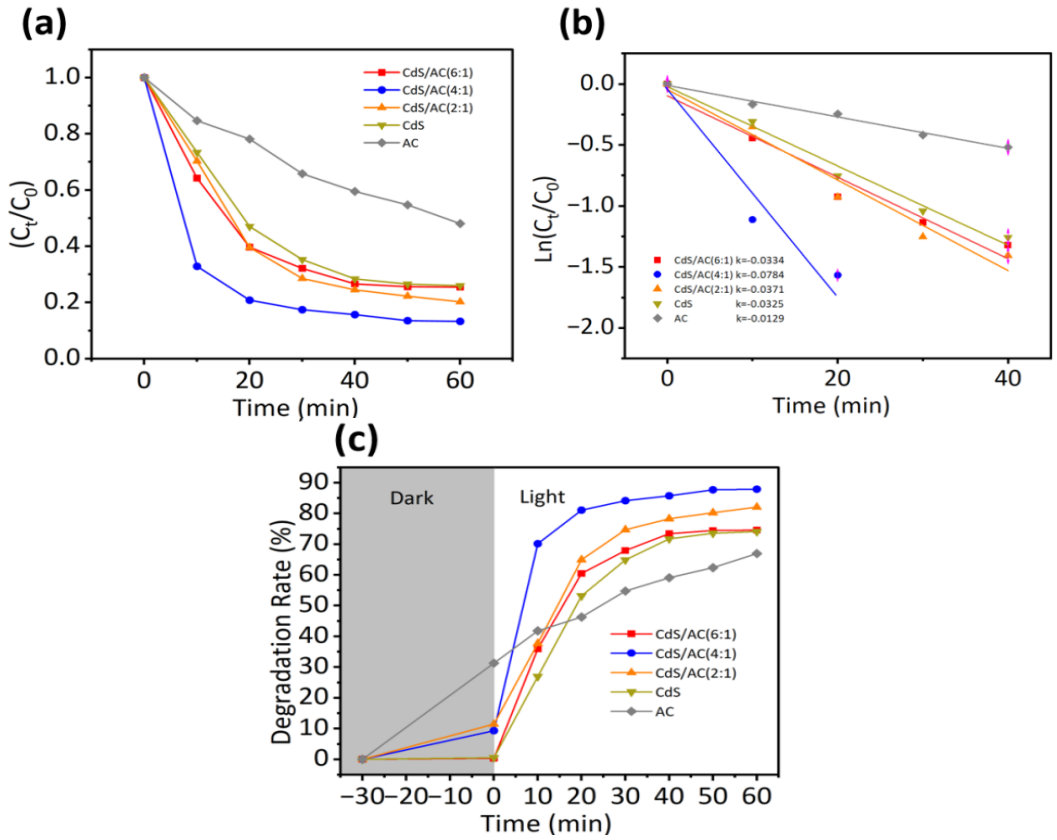

Fig.S2. Change in the proportion of degradation products(a), first-order pseudo-kinetic fitting curve (c), and photo-degradation rate (d) of a 10 mg sample at a contaminant concentration of 20 mg·L^{-1}.

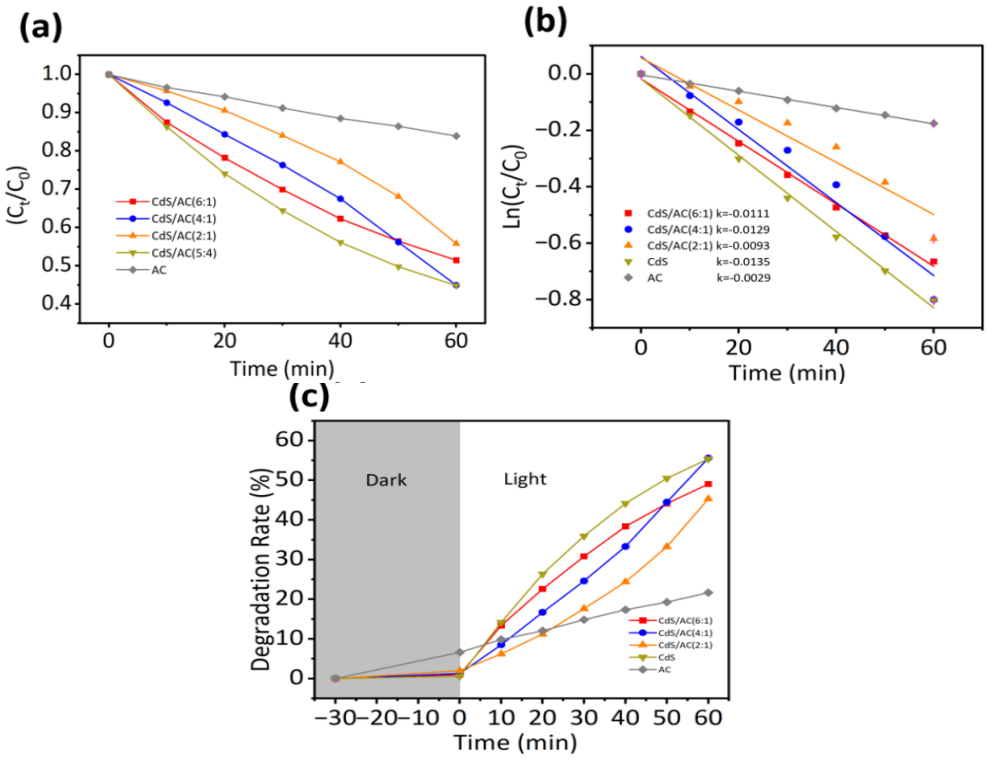

Fig.S3. Change in the proportion of degradation products(a), first-order pseudo-kinetic fitting curve (c), and photo-degradation rate (d) of a 5 mg sample at a contaminant concentration of 40 mg·L^{-1}.

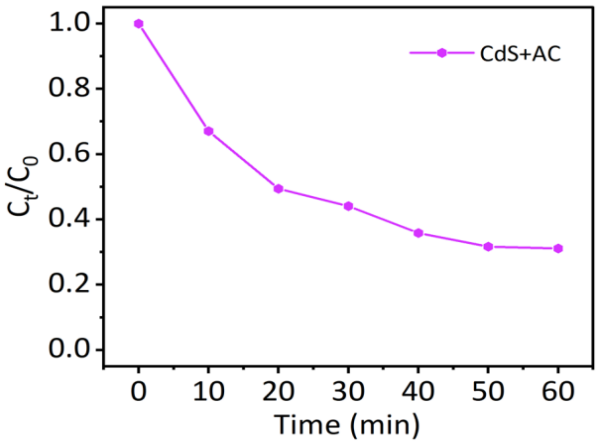

Fig.S4. The mechanical stirring degradation diagram of CdS and AC.

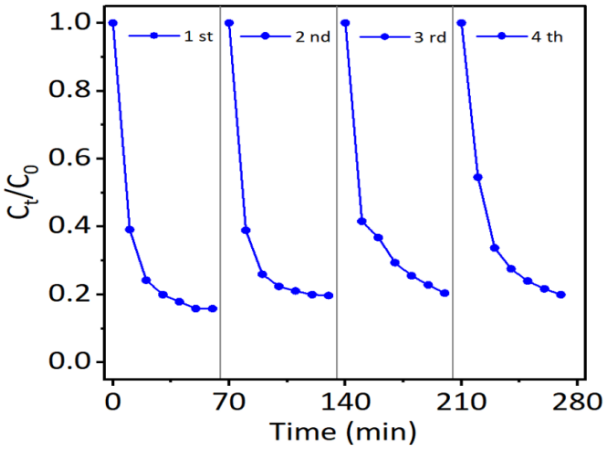

Fig.S5. The stability tests of photocatalytic degradation of CdS/AC(4:1)